Probing Structure in the Polymorphic Domain of the L-Enantiomer of *N*-Benzoyl-Phenylalanine by Means of 2D Solid-State NMR Spectroscopy and DFT Calculations

Colan E. Hughes,*,†,§ Sebastian Olejniczak,‡ Jan Helinski,‡ Włodzimierz Ciesielski,‡ Michal Repisky,‡,# Ovidiu C. Andronesi,† Marek J. Potrzebowski,*,‡ and Marc Baldus*,†

Department for NMR-Based Structural Biology, Max-Planck Institute for Biophysical Chemistry, 37077 Göttingen, Germany, and Centre of Molecular and Macromolecular Studies, Polish Academy of Sciences, Sienkiewicza 112, Łódź, Poland.

Received: July 8, 2005; In Final Form: October 17, 2005

A study of polymorphism using a range of solid-state NMR techniques is presented. We demonstrate the existence of at least six polymorphs in a sample of *N*-benzoyl-L-phenylalanine. We also present methodology for the characterization of the protonation state, hydrogen bonding, and molecular conformation for the polymorphs, together with results of such a characterization for one of the polymorphs present in our sample. DFT modeling is used to investigate the separate effects hydrogen bonding and molecular conformation have on the chemical shift tensor.

Introduction

Polymorphism and pseudo-polymorphism[1,2] together form a major issue for the pharmaceutical industry. The existence of different possible structures, resulting from crystallization from solution, is widespread, causing significant difficulties in terms of drug bioavailability (due to different solubilities) and quality control (due to different spectroscopic responses).[3] Polymorphism is particularly common in flexible molecules possessing different possibilities for hydrogen bonding. Irrespective of whether the different forms have the same solvent contents (true polymorphism) or different contents (pseudo-polymorphism), the presence of more than one crystalline form *in the same sample* presents a great challenge for those attempting sample characterization. Solid-state NMR has been recognized as a useful tool for studying polymorphism.[4−26] However, until now, studies on polymorphic mixtures have largely been restricted to the use of one-dimensional spectra.[6,10,18]

More sophisticated, multidimensional spectroscopic methods have been applied to differentiate separate samples composed of single polymorphs.[9,11,25,26] These have included the use of selective ^{13}C labeling to facilitate conformational analysis[9] and recent studies of protein fibril polymorphs.[25,26] The use of ^{13}C labeling has also recently been demonstrated for studying polymorphism in pharmaceuticals.[27] In our study, we apply a range of hetero- and homonuclear correlation solid-state NMR techniques to a site-specifically labeled, polymorphic sample to identify the existence of different polymorphs and characterize their molecular structure. DFT calculations have also been used in some studies of polymorphism.[12,17] We perform DFT calculations to assess the ability of this method to assist in polymorph characterization.

SCHEME 1. Structure of *N*-benzoyl-phenylalanine

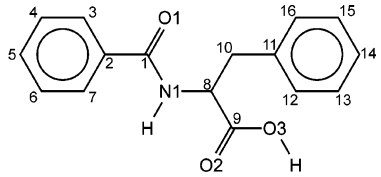

We focus on *N*-benzoyl-phenylalanine (*N*-Bz-Phe), the molecular structure of which is shown in Scheme 1. A racemic mixture crystallizes to give a single form for which a crystal structure has been determined[28] in which two different hydrogen bonds and $\pi-\pi$ interactions are present (see Supporting Information). However, samples containing only one enantiomer do not precipitate into a single crystalline form.[29] Rather, a mixture of different crystalline forms results.[30] Such behavior is not uncommon among amino acids and their derivatives, with both glycine[31,32] and L-glutamic acid[33] being examples of polymorphism which have been investigated by solid-state NMR. The recent application of bortezomib (Velcade), a derivative of *N*-pyrazoyl-phenylalanine, to the treatment of cancer[34,35] demonstrates the practical implications for the pharmaceutical industry for the study of polymorphism of a phenylalanine derivative protected by an aromatic carboxylic acid.

Experimental Section

Two crystalline samples of *N*-Bz-Phe, 99% ^{13}C labeled at the carboxyl and carbonyl positions (C1 and C9, see Scheme 1), were synthesized according to the standard procedure given by Bodanszky et al.,[36] as described in ref 28. Sample **1** was made from pure L-enantiomer, while sample **2** was produced from a racemic mixture. A third sample, **2a**, was prepared from a racemic mixture of *N*-Bz-Phe in which 10% of the molecules were ^{13}C labeled at the C1 and C9 positions.

* To whom correspondence may be addressed. E-mail: hughesce@cardiff.ac.uk, marekpot@bilbo.cbmm.lodz.pl, maba@mpibpc.mpg.de.

† Max-Planck Institute for Biophysical Chemistry.

‡ Polish Academy of Sciences.

§ Present address: School of Chemistry, Cardiff University, Cardiff, CF10 3AT, United Kingdom.

Permanent address: Department of Theoretical Chemistry, Institute of Inorganic Chemistry, Slovak Academy of Sciences, Dubravska cesta 9, SK-845 36, Bratislava, Slovakia.

10.1021/jp053754e CCC: $30.25
Published on Web 11/17/2005

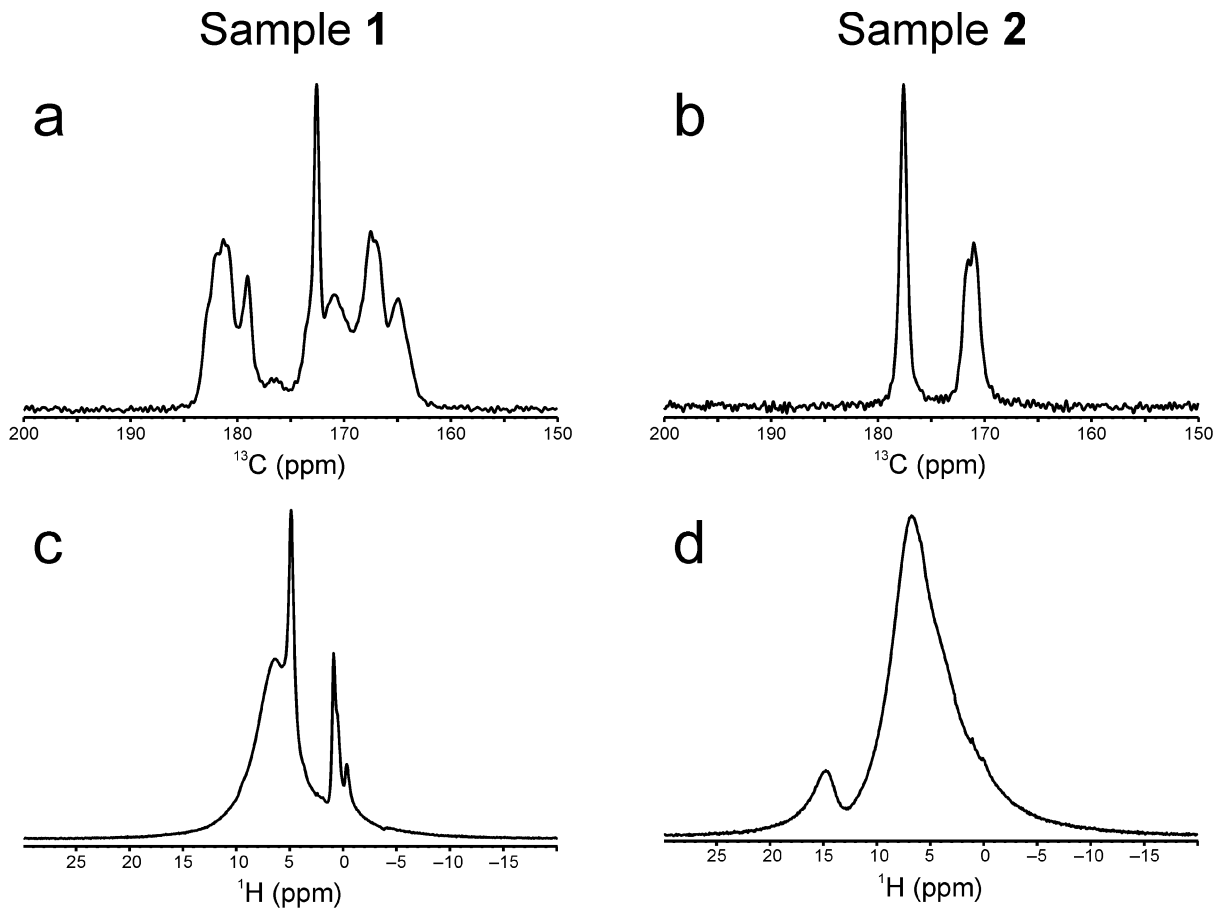

Figure 1. (a)^{13}C CP/MAS spectra of sample **1** recorded with MAS frequency of 8 kHz, B_0 of 7.35 T, 20 °C, and 2 ms cross-polarization contact times. (b) ^{13}C CP/MAS spectra of sample **2** recorded with the same conditions as (a). (c)^{1}H spectrum of **1** recorded with an MAS frequency of 23 kHz, B_0 of 9.4 T, 5 °C, and 3 μs 90° pulses. (d) ^{1}H spectrum of **2** recorded with the same conditions as (c) except an MAS frequency of 25 kHz.

The solid-state CP MAS ^{13}C NMR experiments were performed on Bruker DSX 300, DSX 400, and Avance 600 spectrometers operating at 7, 9.4, and 14.1 T, respectively. The spectrometers were equipped with MAS probeheads for 4-mm and 2.5-mm ZrO_2 rotors. A recycle delay of 3 s was used in all experiments, with ramped cross polarization[37] from ^{1}H nuclei used in all experiments observing ^{13}C signals. Standard, nested phase cycling was used for coherence selection, with TPPI[38] used in all two-dimensional experiments to establish sign discrimination in the indirect dimension. ^{1}H decoupling during data acquisition periods was carried out using on-resonance TPPM.[39] Double-quantum excitation and reconversion was achieved using the POST-C7[40] and SPC5[41] sequences, performed without ^{1}H decoupling.[42] POST-C7 experiments were carried out on DSX 300 and Avance 600 instruments with MAS frequencies of 7 and 12 kHz. The appropriate r.f. pulse nutation frequencies were 49 and 84 kHz. SPC5 experiments were carried out on an Avance 600 instrument with an MAS frequency of 17 kHz and an r.f. nutation frequency of 85 kHz. Double-quantum filtering efficiencies were typically on the order of 3%. CSA recoupling was achieved using the $R10_3^9$ symmetry[43] implemented with a $90°_0270°_{180}$ R element at a spinning speed of 12 kHz and with an r.f. nutation frequency of 40 kHz.

DSC and TGA measurements were carried out on TA instruments 2920 Modulated DSC and Hi-Res TGA 2950 Analyzer. DFT calculations were carried out with the GAUSSIAN 98 program[44] running on a Silicon Graphics Power Challenge computer. The GIAO method[45] was used, with the B3PW91 hybrid functional[46−48] and the basis sets 6-311G** and 6-311++G**,[49,50] to calculate NMR parameters. The SIMPSON program[51] was used to simulate the result of double-quantum filter experiments and CSA recoupling.

NMR Spectroscopy Results

One-Dimensional Spectra. Figure 1 shows ^{13}C and ^{1}H 1D spectra of samples **1** and **2**. The ^{13}C spectra show clear differences. The ^{13}C spectrum of the racemate (Figure 1b) is characterized by two well-resolved resonance lines confirming that only one distinct type of molecule is present. In the case of the L-enantiomer (Figure 1a), the spectrum is rather complex, apparently due to the presence of at least four polymorphs. Figure 1c and d show the ^{1}H NMR spectra of **1** and **2**. The spectrum of **1** (Figure 1c) includes a sharp feature at 5 ppm, not present for sample **2**. This is indicative of nonspecifically absorbed water, the presence of which (2.8 wt %) is confirmed by thermal analysis (TGA and DSC profiles are presented in the Supporting Information). The DCS results suggest the occurrence of crystalline water but we see no clear evidence of crystalline water in the ^{1}H spectrum, which would appear at a higher ppm values (due to hydrogen bonding) and with a broader line shape. Unfortunately, the sample undergoes decomposition above 100 °C, hindering measurement of the crystalline water content.

Two-Dimensional Double-Quantum Spectra. The assignment of the ^{13}C NMR signals for the polymorphs present in sample **1** (Figure 1a) is ambiguous, since the two separate regions of peaks (163−174 ppm and 178−184 ppm) cannot be classified as carbonyl and carboxyl with any certainty. To properly discriminate the signals from the different polymorphs,

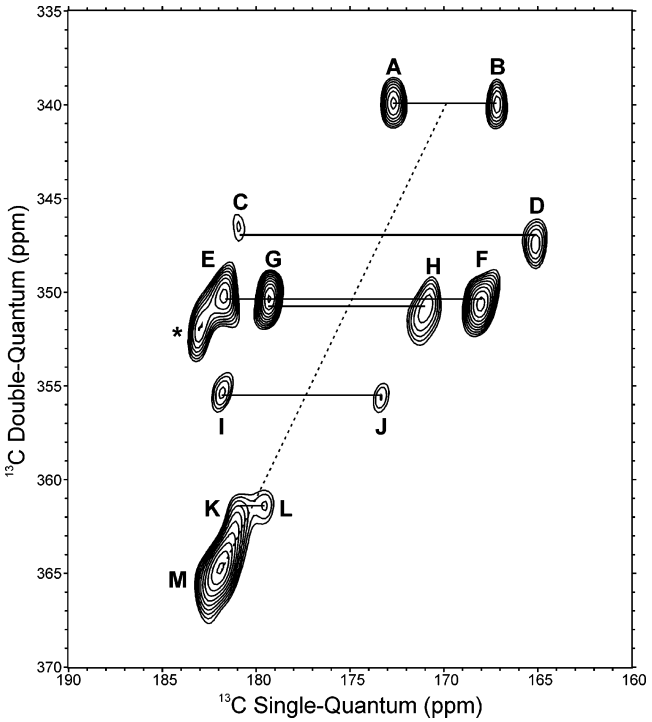

Figure 2. POST-C7 2D correlation spectrum of **1** carried out with $\tau_{exc} = 3$ ms, 12 kHz MAS frequency, B_0 of 14.1 T, and 5 °C. Horizontal lines join correlated resonances, and the dashed line indicates the spectrum diagonal, at a ratio of 2:1. The spectrum was recorded with 100 kHz decoupling during signal acquisition in both t_1 and t_2 but no decoupling during the POST-C7 sequences. A total of 64 t_1 increments were made, with 512 acquisitions per increment.

we have performed a 2D experiment in which the double-quantum ^{13}C spectrum is correlated with single-quantum ^{13}C signals. This spectrum, acquired using the POST-C7 pulse sequence, is shown in Figure 2.

Clear-cut and well-separated peaks are present, with pairs (linked by horizontal lines) corresponding to different polymorphs. Six pairs are labeled by letters (**A**, **B**), (**C**, **D**), etc., and we will henceforth refer to individual polymorphs by the pairs of letters **AB**, **CD**, etc. Two additional peaks are observed. The first, labeled **M**, is at a position corresponding to double-quantum coherence between two ^{13}C resonances with the same chemical shift. The other, labeled *, is of unknown origin. Similar spectra acquired at lower magnetic fields show an additional peak corresponding to double-quantum coherence between two **A** sites, indicating an intermolecular contact. We do not see any intermolecular contacts between members of different pairs. Such interactions would indicate the presence of two conformationally distinct molecules in the asymmetric crystallographic unit. However, we cannot completely rule out the possibility as the longer internuclear distances for such contacts may preclude their observation. The assignment of carboxylic (C9) and carbonyl (C1) positions to members of the pairs remains open to question. This problem may be solved by observing the ^{1}H−^{13}C correlations.

Two-Dimensional HETCOR Spectra. The interactions between ^{1}H and ^{13}C nuclei may be probed using the heteronuclear correlation experiment (HETCOR).[52,53] We have used a sample of the racemate as a reference. Figure 3a shows the carbonyl region of a ^{1}H−^{13}C HETCOR spectrum of sample **2a**. This spectrum allows us to identify three ^{1}H resonances. For the carboxylate (^{13}C shift of 178 ppm), two ^{1}H resonances are present at 5.5 and 14.5 ppm, corresponding to the methine ^{1}H (bonded to C8) and the carboxyl ^{1}H, with the latter shift

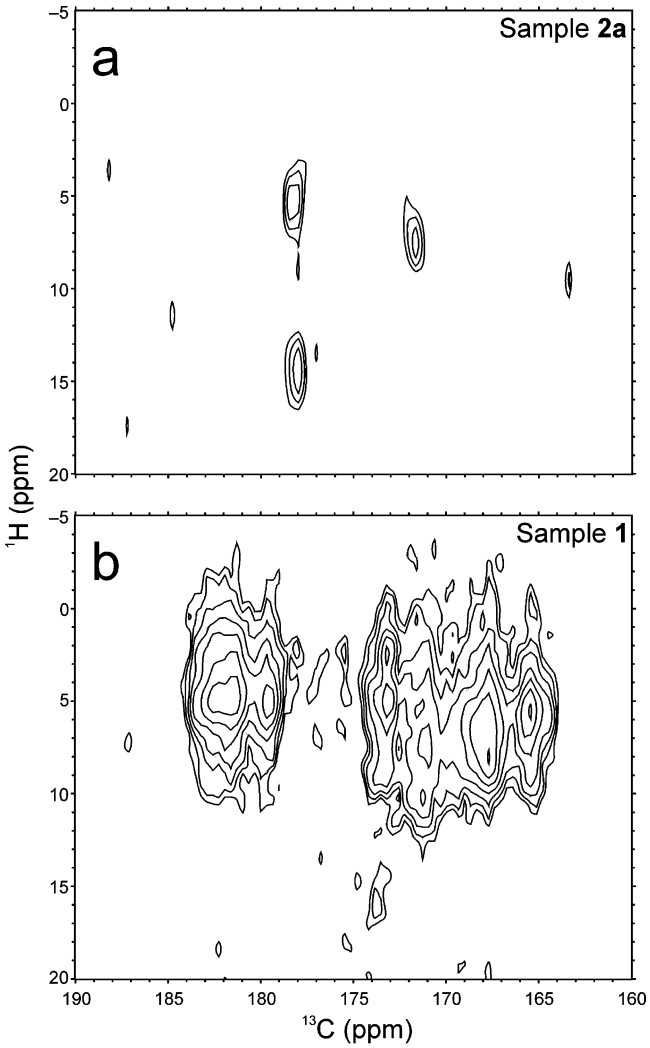

Figure 3. (a) ^{1}H−^{13}C HECTOR spectrum sample **2a** recorded with 1 ms cross-polarization contact time, 23 kHz MAS frequency, B_0 of 9.4 T, and 5 °C. (b) ^{1}H−^{13}C HECTOR spectrum of **1** recorded with 1 ms cross-polarization contact time, 25 kHz MAS frequency, B_0 of 14.1 T, and 5 °C. Both spectra used 1 ms cross-polarization contact times, with 128 t_1 increments and 768 acquisitions per increment.

indicating strong hydrogen bonding. For the carbonyl (^{13}C shift of 171.5 ppm), one ^{1}H resonance is seen at 7.5 ppm, corresponding to the amide ^{1}H and indicating weak hydrogen bonding.

Figure 3b shows the HETCOR spectrum of sample **1**. Resonances **A**, **C**, **E**, **G**, and **I** have a correlation with the ^{1}H resonance at 5.5 ppm, corresponding to the methine carbon adjacent to the carboxyl. This indicates that these sites are carboxyls, allowing us to identify **B**, **D**, **F**, **H**, and **J** as carbonyls. We see a distribution of ^{1}H frequencies for the correlations to the carbonyl peaks, indicating a range of different amide ^{1}H resonances. Most distinct is the ^{1}H resonance at 16 ppm correlating to the **J** site. This corresponds to a strongly hydrogen bonded N−H. We have also carried out a three-dimensional experiment correlating ^{1}H frequencies with ^{13}C double-quantum coherence and ^{13}C single-quantum coherence (not shown). Taking a slice of this 3D spectrum at a ^{1}H frequency of 16 ppm confirms the correlation to the **J** site and not to the **A** site, which has a similar ^{13}C chemical shift.

Chemical Shift Anisotropy Measurements. The chemical shift tensors (CSTs) of carbonyl sites are sensitive to hydrogen bonding and, for carboxyl groups, to the protonation state.[54,55] We have therefore attempted to measure the principal compo-

SCHEME 2: Structures Used in the DFT GIAO Computations, Based on the X-ray Structure of 2

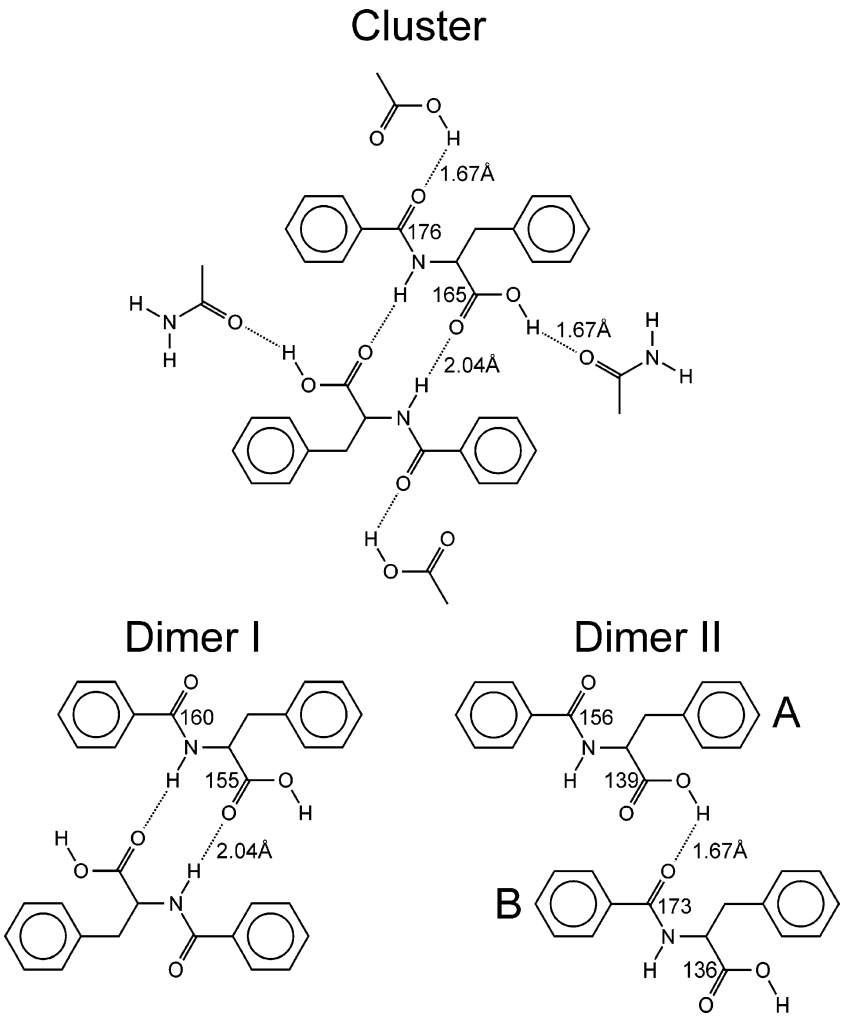

Dimer II consists of two inequivalent molecules, A and B. The O···H distances are shown for the hydrogen bonds (dotted lines), as are the calculated δ_{22} values (in ppm) for C1 and C9.

nents, δ_{ii}, of the CSTs. For rotating solids, the principal components are available from analysis of the spinning sidebands resulting from the modulation of the chemical shift anisotropy (CSA) by macroscopic rotation. For sample **2**, the principal values of the tensors may be extracted from low-speed 1D CP/MAS spectra. However, this method can only give accurate information for peaks which do not overlap in the spectrum, of which there are no cases for sample **1**.

To observe the spinning sidebands in an unambiguous manner, a two-dimensional spectrum in which the peaks are resolved would be preferable. Unfortunately, the spinning sidebands in such spectra are influenced by the method of magnetization transfer being used.[56,57] We have therefore turned to a combination of two-dimensional spectroscopy (for resolution) and CSA dephasing (for measuring the CSA), where the peak positions are given by the dipolar coupled spin pair of interest and the peak intensities are modulated by CSA interactions. We adapted the experiment for generating a 2Q-1Q spectrum by adding, after the reconversion step, a CSA dephasing pulse sequence with the symmetry $R10_3^9$ and an R element of $90°_0270°_{180}$. The pulse sequence is shown in the Supporting Information. By acquiring a set of two-dimensional spectra in which the duration of the CSA dephasing is incremented, a dephasing curve for each resonance can be measured, normalized to the intensity with no CSA dephasing applied.

To test the efficacy of the pulse sequence based on the $R10_3^9$ symmetry, we first applied the sequence to a sample of ($^{13}C_2$)-Glycine without an initial double-quantum filter. The dephasing curve obtained for the carbonyl resonance is in good agreement with a curve simulated using the known CSA tensor[58] and exponential damping with a time constant of 1.25 ms, as shown in the Supporting Information.

For the experiments on *N*-Bz-L-Phe, the double-quantum filtration has different efficiencies for differently oriented crystallites. As this then alters the CSA dephasing relative to a situation where all crystallites have equal magnetization, the full experiment must be simulated, necessitating the simultaneous measurement of the CSAs for both nuclei in each molecule. The internuclear distance must also be taken into account, as must the relative orientation of the two CSA tensors. However, this only leads to one further parameter, since we may assume the orientations of the two CSA tensors relative to the bonds are as shown in Scheme 3.

From the spectra that we have measured, only for the molecule **GH** could both dephasing curves (shown in Figure 4) be accurately measured without problems due to overlap from other peaks or weak signal. Hence, only for this polymorph could CSA values be determined. In the case of molecule **AB**, the dephasing experiments revealed that **A** in fact contains two overlapping components with different CSAs, making measurement of the dephasing curve impossible. The best fitting

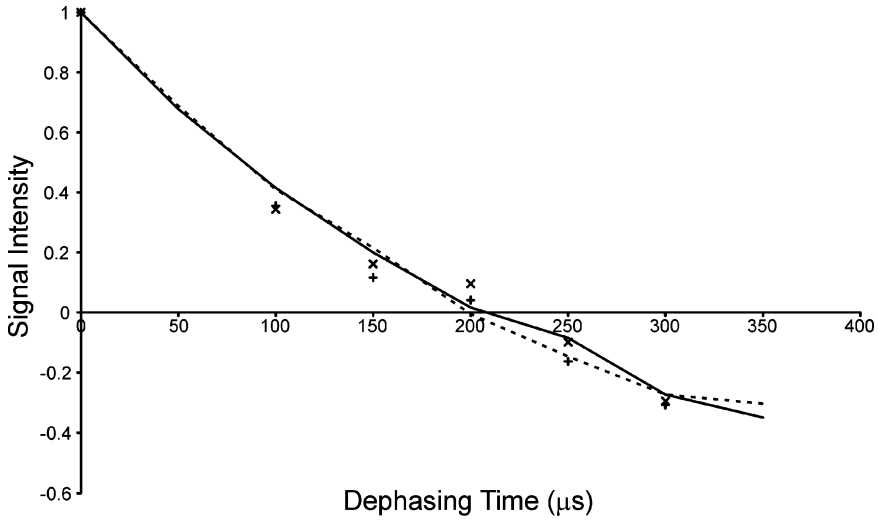

Figure 4. Comparison of experimental CSA dephasing curves for **G** (×) and **H** (+) with the best fitting simulated curves, solid line for **G** and dashed line for **H**. The data were acquired with $\tau_{exc} = 3$ ms, 12 kHz MAS frequency, B_0 of 14.1 T, and 5 °C.

TABLE 1: Chemical Shift Tensors Determined by CSA Dephasing Measurements[a]

sample	polymorph	site	δ_{iso} [ppm]	δ_{aniso} [ppm]	η	δ_{11} [ppm]	δ_{22} [ppm]	δ_{33} [ppm]
1	GH	C9 (COO)	179.1	140	0.5	74.1	144.1	319.1
				−140	0.5	284.1	214.1	39.1
		C1 (CO)	170.6	120	0.2	98.6	122.6	290.6
				−120	0.2	242.6	218.6	50.6
2		C9 (COO)	177.6	83.1	0.67	258.9	164.2	109.7
		C1 (CO)	171.5	−85.0	0.68	242.9	185.1	86.5

[a] Double-quantum build-up curves suggest that δ_{aniso} is positive for both C1 and C9 in **GH**.

SCHEME 3: Standard Orientation of the ^{13}C Principal Elements of the Chemical Shift Tensor with Respect to the Bond Geometry in Carbonyl and Carboxyl Groups

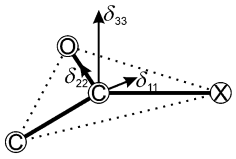

simulated dephasing curves for **G** and **H** are also shown in Figure 4, generated using the SIMPSON program.[51] (A representative input file is included in the Supporting Information.) The parameters for this best fit are $\delta_{aniso}(\mathbf{G}) = \pm 140$ ppm, $\eta(\mathbf{G}) = 0.5$, $\delta_{aniso}(\mathbf{H}) = \pm 120$ ppm, $\eta(\mathbf{H}) = 0.2$, and $d(\mathbf{G}-\mathbf{H}) = 3.2$ Å. Note that, as evolution under $R10_3^9$ with R element $90°_0270°_{180}$ is insensitive to the sign of δ_{aniso}, our fit only provides measurement of the magnitude of the two values of δ_{aniso}. Because of this sign insensitivity, there are two possible values for each of the δ_{ii} components for sites **G** and **H**, as shown in Table 1. As discussed later, the values of δ_{22} for **GH** suggest that the carboxyl is in a non-hydrogen-bonded state, although the sign ambiguity leaves us at this point unable to determine its protonation state.

Although we cannot measure accurate dephasing curves, all the other peaks, with the exception of one of the two components in peak **A**, pass through zero with between 200 and 300 μs of dephasing. This suggests that they have magnitudes of δ_{aniso} similar to those for **G** and **H**. The remaining component dephases more slowly, indicating a smaller value of δ_{aniso}.

Double-Quantum Build-Up Curves. Having arrived at an estimate for the internuclear distance for the polymorph **GH**, we can compare this to the results of an experiment designed to measure such distances. This can be achieved by comparing the build-up curves of the 2Q signals (as in the 2D spectrum in Figure 2) to simulations, using the observed values of the CSTs. To optimize sensitivity of the experiments to the distances, these experiments were performed at a B_0 of 7 T, where the chemical shift is smaller. None the less, significant effects can be expected from the large CSAs and these must be taken into account.

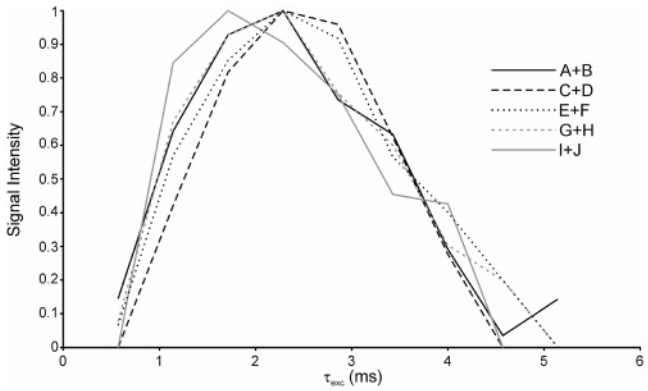

Figure 5. Build-up curves for the intensity of the double-quantum signal due to the different polymorphs in sample **1**. The curves were calculated from spectra acquired at 7 kHz MAS frequency, B_0 of 7 T, and 5 °C.

Figure 5 shows the experimental build-up curves, obtained from spectra acquired using the POST-C7 sequence[40] without ^1H decoupling.[42] The curves have different shapes, with the peak intensity occurring at excitation times, τ_{exc} (equal to reconversion times), of either 1.7 or 2.3 ms. Simulations have been carried out with the SIMPSON program using the values of the CSTs and distance, determined as described above, for the polymorph **GH**. There are four different possibilities due to both values of δ_{aniso} having undetermined signs. Simulations for all four possibilities are near identical for $\tau_{exc} < 2.5$ ms. The simulation with both anisotropies having a positive sign is shown in Figure 6 (together with the experimental data), since this fits the later

TABLE 2: DFT GIAO Chemical Shift Tensors Calculated with the B3PW91 Hybrid Functional and the 6-311G Basis Set[a]**

site	geometry	δ_{iso} [ppm]	δ_{aniso} [ppm]	η	δ_{11} [ppm]	δ_{22} [ppm]	δ_{33} [ppm]
C9 (COO)	optimized	180.8	107.4	0.21	288.2	138.3	115.9
	X-ray	171.6	102.3	0.30	273.9	135.7	105.3
	cluster	177.2	84.4	0.72	261.6	165.2	104.7
	dimer I	178.3	94.9	0.51	273.2	155.1	106.5
	dimer IIA	171.7	95.1	0.32	266.8	139.3	108.9
	dimer IIB	171.4	102.0	0.31	273.5	136.2	104.7
C1 (CO)	optimized	169.7	90.8	0.74	260.5	157.8	90.8
	X-ray	167.7	88.3	0.80	256.1	158.9	88.2
	cluster	169.3	−82.1	0.85	245.2	175.6	87.1
	dimer I	167.3	87.3	0.83	254.6	159.9	87.3
	dimer IIA	166.3	88.0	0.77	254.2	156.3	88.2
	dimer IIB	168.9	−81.0	0.90	245.8	173.1	87.9

[a] Only carboxyl and carbonyl groups are shown.

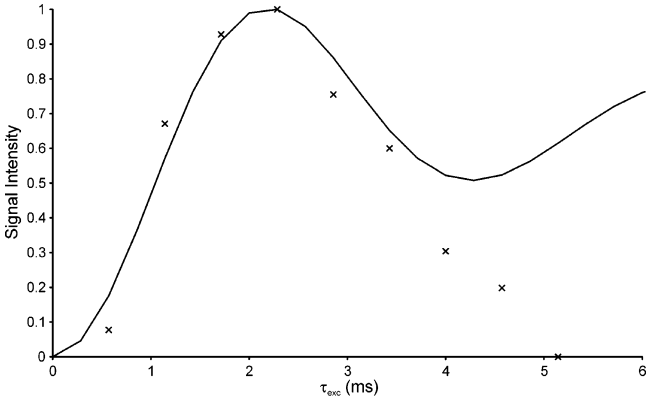

Figure 6. Simulated double-quantum build-up curve for the polymorph **GH**, using the parameters found from fitting the CSA dephasing curve.

points in the experimental data ($\tau_{exc} > 2.5$ ms) somewhat better than the other three. However, all four simulations require additional damping to be brought into good agreement for these later time points. Taking this combination of signs would lead to the conclusion that the carboxyl group in polymorph **GH** is in a deprotonated state.

DFT Results

To gain further insight into the problem of polymorphism of *N*-Bz-L-Phe, we performed DFT calculations of ^{13}C NMR shielding parameters for different structural forms of sample **1**. First, six different molecular geometries were considered, chosen to demonstrate the effects of the different possible hydrogen bonds. In all cases, the positions of the H atoms were established by energy minimization, using the B3PW91 hybrid functional and the 6-311++G** basis set. In the first, the molecular conformation for the L-enantiomer in the X-ray structure of the racemate was taken. In the second, the lowest energy structure for an isolated molecule of *N*-Bz-L-Phe was used. The third geometry took a pair of molecules from the racemate crystal structure and added small molecules to mimic the other hydrogen bonds known from the X-ray structure, as illustrated in Scheme 2. Finally, two dimeric constructions were considered, again based on the X-ray structure. In the first, the molecules were those connected by two amide-to-carboxyl hydrogen bonds, as in the cluster. In the second, the molecules were those linked by a single carboxyl to carbonyl hydrogen bond.

The DFT calculations performed provide values for σ_{11}, σ_{22}, and σ_{33} relative to a free ^{13}C atom. Following Birn et al.,[59] these may be converted to δ_{11}, δ_{22}, and δ_{33} values relative to TMS by subtracting the shielding values from 184.1 ppm, the experimentally determined chemical shift of free ^{13}C atoms.[60] This gives a very good match between the values calculated using the cluster geometry and those measured for the racemate. Table 2 presents the shielding parameters computed for the cluster and dimers shown in Scheme 2.

There are substantial differences between the geometries of the X-ray structure and that generated by energy optimization of an isolated molecule, with, for examples, the C1−N1−C8−C9 torsional angle changing from 61° to 123° (see Supporting Information). To investigate the effect of this one angle, a second group of structures was generated by taking the X-ray structure of an isolated molecule, fixing the C1−N1−C8−C9 torsional angle to a particular value, then optimizing the rest of the structure. The calculated values of δ_{22} vary by up to 17 ppm as the torsional angle varies (see Supporting Information). In one small range of conformations, those with C1−N1−C8−C9 torsional angles of 290° to 295°, an intramolecular hydrogen bond forms between the carboxyl and carbonyl groups. This has a large influence on the NMR parameters, in particular raising the value of δ_{22} by more than 30 ppm, resulting in very similar isotropic chemical shift values for the C1 and C9 sites.

Discussion

An earlier study[30] of *N*-Bz-L-Phe identified the presence of four polymorphs based on the one-dimensional ^{13}C NMR spectrum. Our 2Q-1Q spectrum (Figure 2) has enabled us to identify a minimum of six different polymorphs with at least one distinct C1 or C9 ^{13}C resonance frequency. The identification of such a degree of structural complexity demonstrates the power of this experiment in the study of polymorphism in a single sample. We have sought to characterize the different polymorphs by carrying out experiments which are sensitive to the chemical shift anisotropies of the C1 and C9 sites and the C1−C9 distance. Using a series of two-dimensional correlation spectra, CSA values could be determined for the polymorph **GH**. Due to spectral overlap and spectroscopic insensitivity, a CSA analysis of the other spins could only be performed qualitatively.

A previous solid-state NMR study of carbonyl groups in peptides[54] found values for the magnitude of δ_{aniso} for ^{13}C in the range 75−85 ppm. Elsewhere,[55] values for amino acid carboxyl groups in the range 60−80 ppm for the deprotonated state and 60−90 ppm for the protonated state were reported. Thus, our estimates for the values of δ_{aniso} for sites **G** and **H** fall well outside of the previously observed range. However, neither of these studies considered phenylalanine residues and all were made on crystallized samples which did not exhibit signs of polymorphism. We find no combination of CSA and distance parameters which reproduces the general features of the CSA dephasing and the double-quantum build-up curves assuming magnitudes of δ_{aniso} for both C1 and C9 smaller than

120 ppm. As we do not observe unusually large values for the anisotropy of the racemic sample we conclude that the large values are a feature of some aspect of the poorly crystallized state of our sample.

In contrast to Cα[59] and amide nitrogens,[61] the arrangement of the principal axes of the CST in carbonyl and carboxyl groups are known to adopt a relatively limited range of orientations, around that shown in Scheme 3.[62] In both cases, the δ_{22} component is approximately collinear with the C═O bond. Correlations have been observed, for both carboxyl groups and carbonyl groups in peptide bonds, between the δ_{22} component and the hydrogen bond to the C═O group.[54,55,63] The values of δ_{22} for the racemate (Table 1) suggest that both C1 and C9 act as hydrogen bond acceptors, as is known to be the case from the X-ray structure. From the CSA dephasing measurements, we have two possible values for each δ_{22} in the polymorph **GH**, while our double-quantum build-up curves suggest that δ_{aniso} is positive for both sites. For C9 (carboxyl), the values suggest a non-hydrogen bonded state, either protonated (the lower value) or deprotonated (the higher, indicated by the double-quantum build-up curves). For C1 (carbonyl), the two possible values fall either side of the range previously observed for such groups in the solid state. However, these observations were restricted to alanine and glycine residues,[54] whereas our molecule is based upon phenylalanine.

Due to spectral overlap or weak signal in the 2Q-1Q spectrum, CSA values could not be measured accurately for the polymorphs **AB**, **CD**, **EF**, **IJ**, and **KL**. Nevertheless, the following conclusions can be drawn: (i) The polymorph **AB**, apparently clearly defined from the spectrum in Figure 2, in fact contains two polymorphs, distinguished by the CSA of the carboxyl. These carboxyl resonances are separate from those observed in the other polymorphs. (ii) Polymorphs **CD** and **EF** have somewhat slower double-quantum build-up curves than **GH**, suggesting either a longer internuclear distance or smaller values of δ_{aniso}. (iii) The polymorph **IJ** possesses two notable distinctions. First, we see evidence for hydrogen bonding to the carbonyl group (**J**). Second, we observe a significantly earlier maximum in the experimental double-quantum build-up curve than for **GH**, indicating either a shorter distance or larger values of δ_{aniso}. (iv) Finally, the polymorph **KL** exhibits a very high isotropic chemical shift for the carbonyl.

The orientations of the CSTs calculated by DFT closely match that shown in Scheme 3. The δ_{22} values for the clusters and dimers (Table 2) conform to expectations from previous studies, given the hydrogen bonding present. In particular, the values calculated for the cluster (based on the X-ray structure of the racemate) quite closely match those found experimentally for the racemate. However, none of the calculations, with or without hydrogen bonding, match the magnitude of δ_{aniso} observed for both sites in polymorph **GH**, nor do any give values for δ_{22} close to those observed. The closest is that consisting of a single molecule whose structure has been energetically optimized.

Conclusions

We have identified the presence of at least six polymorphs of *N*-Bz-L-Phe in sample **1**. For one of these polymorphs, we have measured the chemical shift tensors for the labeled sites and the distance between these sites. The magnitudes of the chemical shift anisotropies are larger than those previously measured for similar sites. DFT GIAO theoretical calculations have enabled us to further probe the influence of hydrogen bonding and molecular conformation on the CSTs, allowing us to confirm the previously observed correlation between the δ_{22} component of the ^{13}C chemical shift and the hydrogen bonding to carbonyl and carboxyl sites. However, while the DFT calculation for a cluster of molecules matches quite well to experimental results for the racemate, none of the conformations considered in the DFT calculations give a good match to the experimental values for the polymorph **GH**.

It is apparent from this work that advanced solid-state NMR methodology is a source of unique insight into the complexities of polymorphic samples. There are a number of efforts to introduce theoretical methods enabling the prediction of crystal structures.[64] As discussed in the cited paper, this problem is very difficult even for a single molecular entity. The situation is even more complex for polymorphs, although there are recent reports showing the application of modeling to polymorphism.[65,66] It seems that a joint approach combining theoretical methods supported by constraints obtained from solid-state NMR measurements traces the future for structural studies of polymorphs. Several applications of this approach to samples of this nature composed of a single crystalline form have already appeared.[67−69]

Acknowledgment. We are grateful to the Committee for Scientific Research, MNiI, grant 3 T09A 173 27. The financial support of the European Commission within the fifth Framework Program (Contract ICA1-CT-2000-70021 − Centres of Excellence) is gratefully acknowledged. This work was also in part funded by the DFG and an Alexander-von-Humboldt postdoctoral fellowship for C. E. H. S. O. is the holder of a Domestic Grant for Young Scientists from the Foundation for Polish Science. Krisztina Fehér and Henrike Heise are thanked for experimental assistance.

Supporting Information Available: Figures of intermolecular contacts of **2**, DSC profiles of **2** and **1**, TGA profile of **1**, pulse sequence for acquiring CSA dephasing curves, and CSA dephasing curve for glycine; tables of geometrical parameters and DFT GIAO chemical shift tensors; and SIMPSON program. This material is available free of charge via the Internet at http://pubs.acs.org.

References and Notes

(1) Glusker, J. P.; Lewis, M.; Rossi, M. *Crystal Structure Analysis for Chemists and Biologists*; VCH Publishers: New York, 1994.
(2) Caira, M. R. *Top. Curr. Chem.* **1998**, *198*, 163.
(3) Bernstein, J. *Polymorphism in Molecular Crystals*; Oxford University Press: New York, 2002.
(4) Harris, R. K. Polymorphism and Related Phenomena. In *Encyclopedia of Nuclear Magnetic Resonance*; Grant, D. M., Harris, R. K., Eds.; Wiley: Chichester, 1996; p 3734.
(5) Smith, J.; MacNamara, E.; Raftery, D.; Borchardt, T.; Byrn, S. *J. Am. Chem. Soc.* **1998**, *120*, 11710.
(6) Padden, B. E.; Zell, M. T.; Dong, Z.; Schroeder, S. A.; Grant, D. J. W.; Munson, E. J. *Anal. Chem.* **1999**, *71*, 3325.
(7) Beckmann, P. A.; Burbank, K. S.; Clemo, K. M.; Slonaker, E. N.; Averill, K.; Dybowski, C.; Figueroa, J. S.; Glatfelter, A.; Koch, S.; Liable-Sands, L. M.; Rheingold, A. L. *J. Chem. Phys.* **2000**, *113*, 1958.
(8) Henck, J.-O.; Finner, E.; Burger, A. *J. Pharm. Sci.* **2000**, *89*, 1151.
(9) Middleton, D. A.; Duff, C. S. L.; Peng, X.; Reid, D. G.; Saunders, D. *J. Am. Chem. Soc.* **2000**, *122*, 1161.
(10) Variankaval, N. E.; Jacob, K. I.; Dinh, S. M. *J. Cryst. Growth* **2000**, *217*, 320.
(11) Zell, M. T.; Padden, B. E.; Grant, D. J. W.; Schroeder, S. A.; Wachholder, K. L.; Prakash, I.; Munson, E. J. *Tetrahedron* **2000**, *56*, 6603.
(12) Strohmeier, M.; Orendt, A. M.; Alderman, D. W.; Grant, D. M. *J. Am. Chem. Soc.* **2001**, *123*, 1713.
(13) Dong, Z.; Padden, B. E.; Salsbury, J. S.; Munson, E. J.; Schroeder, S. A.; Prakash, I.; Grant, D. J. W. *Pharm. Res.* **2002**, *19*, 330.
(14) Harper, J. K.; Facelli, J. C.; Barich, D. H.; McGeorge, G.; Mulgrew, A. E.; Grant, D. M. *J. Am. Chem. Soc.* **2002**, *124*, 10589.
(15) Maurin, M. B.; Vickery, R. D.; Rabel, S. R.; Rowe, S. M.; Everlof, J. G.; Nemeth, G. A.; Campbell, G. C.; Foris, C. M. *J. Pharm. Sci.* **2002**, *91*, 2599.

(16) Morzycki, J. W.; Wawer, I.; Gryszkiewicz, A.; Maj, J.; Siergiejczyk, L.; Zaworska, A. *Steroids* **2002**, *67*, 621.
(17) Novoselsky, A.; Glaser, R. *Magn. Reson. Chem.* **2002**, *40*, 723.
(18) Sidhu, P. S.; Enright, G. A.; Ripmeester, J. A.; Penner, G. H. *J. Phys. Chem. B* **2002**, *106*, 8569.
(19) Tishmack, P. A.; Bugay, D. E.; Byrn, S. R. *J. Pharm. Sci.* **2003**, *92*, 441.
(20) Potrzebowski, M. J. *Eur. J. Org. Chem.* **2003**, *2003*, 1367.
(21) Agrawal, S.; Ashokraj, Y.; Bharatam, P. V.; Pillai, O.; Panchagnula, R. *Eur. J. Pharm. Sci.* **2004**, *22*, 127.
(22) Booy, K.-J.; Wiegerinck, P.; Vader, J.; Kaspersen, F.; Lambregts, D.; Vromans, H.; Kellenbach, E. *J. Pharm. Sci*. **2005**, *94*, 458.
(23) Rubin-Preminger, J. M.; Bernstein, J.; Harris, R. K.; Evans, I. R.; Ghi, P. Y. *Cryst. Growth Des.* **2004**, *4*, 431.
(24) Rubin-Preminger, J. M.; J.Bernstein; Harris, R. K.; Evans, I. R.; Ghi, P. Y. *J. Pharm. Sci.* **2004**, *93*, 2810.
(25) Petkova, A. T.; Leapman, R. D.; Guo, Z.; Yau, W.-M.; Mattson, M. P.; Tycko, R. *Science* **2005**, *307*, 262.
(26) Heise, H.; Hoyer, W.; Becker, S.; Andronesi, O. C.; Riedel, D.; Baldus, M. *Proc. Natl. Acad. Sci., U. S. A.* **2005**, *102*, 15871.
(27) Booy, K.-J.; Wiegerinck, P.; Vader, J.; Kaspersen, F.; Lambregts, D.; Vromans, H.; Kellenbach, E. *J. Pharm. Sci*. **2004**, *94*, 458.
(28) Potrzebowski, M. J.; Tekely, P.; Wieczorek, M. W.; Blaszczyk, J. *J. Pept. Res.* **2000**, *56*, 185.
(29) Chu, P. J.; Potrzebowski, M. J.; Gao, Y. D.; Scott, A. I. *J. Am. Chem. Soc.* **1990**, *112*, 881.
(30) Potrzebowski, M. J.; Schneider, C.; Tekely, P. *Chem. Phys. Lett.* **1999**, *313*, 569.
(31) Potrzebowski, M. J.; Tekely, P.; Dusausoy, Y. *Solid State Nucl. Magn. Reson.* **1998**, *11*, 253.
(32) Gu, Z.; Ebisawa, K.; McDermott, A. *Solid State Nucl. Magn. Reson.* **1996**, *7*, 161.
(33) Kitchin, S. J.; Ahn, S. B.; Harris, K. D. M. *J. Phys. Chem. A* **2002**, *106*, 7228.
(34) Schenkein, D. *Clin. Lymphoma* **2002**, *3*, 49.
(35) Albanell, J.; Adams, J. *Drugs Future* **2002**, *27*, 1079.
(36) Bodaszansky, M.; Bodaszansky, A. *The Practice of Peptide Synthesis*; Akademie Verlag: Berlin, 1985.
(37) Metz, G.; Wu, X. L.; Smith, S. O. *J. Magn. Reson.* **1994**, *A 110*, 219.
(38) Ernst, R. R.; Bodenhausen, G.; Wokaun, A. *Principles of Nuclear Magnetic Resonance in One and Two Dimensions*; Clarendon Press: Oxford, 1987.
(39) Bennett, A. E.; Rienstra, C. M.; Auger, M.; Lakshmi, K. V.; Griffin, R. G. *J. Chem. Phys.* **1995**, *103*, 6951.
(40) Hohwy, M.; Jakobsen, H. J.; Edén, M.; Levitt, M. H.; Nielsen, N. C. *J. Chem. Phys.* **1998**, *108*, 2686.
(41) Hohwy, M.; Rienstra, C. M.; Jaroniec, C. P.; Griffin, R. G. *J. Chem. Phys.* **1999**, *110*, 7983.
(42) Hughes, C. E.; Luca, S.; Baldus, M. *Chem. Phys. Lett.* **2004**, *385*, 435.
(43) Levitt, M. H. Symmetry-Based Pulse Sequences in Magic-Angle Spinning Solid-State NMR. In *Encyclopedia of Nuclear Magnetic Resonance: Supplementary Volume*; Harris, R. K., Ed.; Wiley: Chichester, 2002; p 165.
(44) Frisch, M. J.; Trucks, G. W.; Schlegel, H. B.; Scuseria, G. E.; Robb, M. A.; Cheeseman, J. R.; Zakrzewski, V. G.; Montgomery, J. A.; Stratmann, R. E.; Burant, J. C.; Dapprich, S.; Millam, J. M.; Daniels, A. D.; Kudin, K. N.; Strain, M. C.; Farkas, O.; Tomasi, J.; Barone, V.; Cossi, M.; Cammi, R.; Mennucci, B.; Pomelli, C.; Adamo, C.; Clifford, S.; Ochterski, J.; Petersson, G. A.; Ayala, P. Y.; Cui, Q.; Morokuma, K.; Malick, D. K.; Rabuck, A. D.; Raghavachari, K.; Foresman, J. B.; Cioslowski, J.; Ortiz, J. V.; Stefanov, B. B.; Liu, G.; Liashenko, A.; Piskorz, P.; Komaromi, I.; Gomperts, R.; Martin, R. L.; Fox, D. J.; Keith, T.; Al-Laham, M. A.; Peng, C. Y.; Nanayakkara, A.; Gonzalez, C.; Challacombe, M.; Gill, P. M. W.; Johnson, B.; Chen, W.; Wong, M. W.; Andres, J. L.; Gonzalez, C.; Head-Gordon, M.; Replogle, E. S.; Pople, J. A. Gaussian 98; Revision A.6 ed.; Gaussian, Inc: Pittsburgh, PA, 1998.
(45) Ditchfield, R. *J. Chem. Phys.* **1972**, *56*, 5688.
(46) Perdew, J. P.; Wang, Y. *Phys. Rev. B* **1992**, *45*, 13244.
(47) Becke, A. D. *J. Chem. Phys.* **1993**, *98*, 1372.
(48) Becke, A. D. *J. Chem. Phys.* **1993**, *98*, 5648.
(49) Krishnan, R.; Binkley, J. S.; Seeger, R.; Pople, J. A. *J. Chem. Phys.* **1980**, *72*, 650.
(50) Frisch, M. J.; Pople, J. A.; Binkley, J. S. *J. Chem. Phys.* **1984**, *80*, 3265.
(51) Bak, M.; Rasmussen, J. T.; Nielsen, N. C. *J. Magn. Reson.* **2000**, *147*, 296.
(52) Caravatti, P.; Bodenhausen, G.; Ernst, R. R. *Chem. Phys. Lett.* **1982**, *89*, 363.
(53) Caravatti, P.; Braunschweiler, L.; Ernst, R. R. *Chem. Phys. Lett.* **1983**, *100*, 305.
(54) Wei, Y. F.; Lee, D. K.; Ramamoorthy, A. *J. Am. Chem. Soc.* **2001**, *123*, 6118.
(55) Gu, Z.; Zambrano, R.; McDermott, A. E. *J. Am. Chem. Soc.* **1994**, *116*, 6368.
(56) Tycko, R.; Berger, A. E. *J. Magn. Reson.* **1999**, *141*, 141.
(57) Tycko, R.; Weliky, D. P.; Berger, A. E. *J. Chem. Phys.* **1996**, *105*, 7915.
(58) Haberkorn, R. A.; Stark, R. E.; H, V. W.; Griffin, R. G. *J. Am. Chem. Soc.* **1981**, *103*, 2534.
(59) Birn, J.; Poon, A.; Mao, Y.; Ramamoorthy, A. *J. Am. Chem. Soc.* **2004**, *126*, 8529.
(60) Jameson, A. K.; Jameson, C. J. *Chem. Phys. Lett.* **1987**, *134*, 461.
(61) Poon, A.; Birn, J.; Ramamoorthy, A. *J. Phys. Chem. B* **2004**, *108*, 16577.
(62) Veeman, W. S. *Prog. Nucl. Magn. Reson. Spectrosc.* **1984**, *16*, 193.
(63) Gu, Z.; McDermott, A. E. *J. Am. Chem. Soc.* **1993**, *115*, 4282.
(64) Motherwell, W. D. S.; Ammon, H. L.; Dunitz, J. D.; Dzyabchenko, A.; Erk, P.; Gavezzotti, A.; Hofmann, D. W. M.; Leusen, F. J. J.; Lommerse, J. P. M.; Mooij, W. T. M.; Price, S. L.; Scheraga, H.; Schweizer, B.; Schmidt, M. U.; Eijck, B. P. v.; Verwer, P.; Williams, D. E. *Acta Crystallogr., Sect. B: Struct. Sci.* **2002**, *58*, 647.
(65) Gavezzotti, A. *CrystEngComm* **2002**, *4*, 343.
(66) Mattheus, C. C.; de Wijs, G. A.; de Groot, R. A.; Palstra, T. T. M. *J. Am. Chem. Soc.* **2003**, *125*, 6323.
(67) Harris, R. K. *Solid State Si.* **2004**, *6*, 1025.
(68) Elen, B.; Emsley, L. *J. Am. Chem. Soc.* **2005**, *127*, 9140.
(69) Brouwer, D. H.; Darton, R. J.; Morris, R. E.; Levitt, M. H. *J. Am. Chem. Soc.* **2005**, *127*, 10365.